Journal of Power Sources 217 (2012) 509–518

Contents lists available at SciVerse ScienceDirect

Journal of Power Sources

journal homepage: www.elsevier.com/locate/jpowsour

Electro-thermal cycle life model for lithium iron phosphate battery

Yonghuang Ye [a], Yixiang Shi [b], Andrew A.O. Tay [a,*]

[a] Department of Mechanical Engineering, National University of Singapore, 9 Engineering Drive 1, Singapore 117576, Singapore
[b] Key Laboratory for Thermal Science and Power Engineering of Ministry of Education, Tsinghua University, Beijing 100084, China

HIGHLIGHTS

- An electro-thermal cycle life model of lithium ion battery accounting for thermal and capacity fading effects.
- Comprehensive model calibrations and validations.
- Effects of temperature on capacity fading rate.
- Two effective methods for capacity fade recover of cycled battery.

ARTICLE INFO

Article history:
Received 28 March 2012
Received in revised form
11 June 2012
Accepted 13 June 2012
Available online 23 June 2012

Keywords:
Lithium ion battery
Electro-thermal model
Capacity fading
OCV
Capacity recover

ABSTRACT

An electro-thermal cycle life model is developed by incorporating the dominant capacity fading mechanism to account for the capacity fading effect on the lithium ion battery performance. This model is comprehensively validated in three different aspects: (1) Electrochemical performance with different discharge *C*_rates (C/10, 1C, 3C) and different ambient temperature (0 °C, 25 °C, 45 °C, 60 °C); (2) battery surface temperature and center temperature during 6 *C*_rate constant current charge–constant voltage charge–constant current discharge (CC–CV–CC); (3) the amount of capacity fade indicated by the discharge potential curves of different cycle conditions. The feasibility of using the dominant factor only to represent the overall capacity fading in model is verified, and the model is used to predict OCV–SOC curves of cycled battery. To recover the capacity fade of cycled battery, either charging the negative electrode of fully discharged battery or charging the positive electrode of fully charged battery, could be an effective method, and possible capacity recovering design is presented. The decreasing trend of thermodynamic parameter E_a with increasing *C*_rate in the capacity fading function is deduced with increasing battery temperature when increasing discharge *C*_rate.

1. Introduction

Growing concerns have been paid on the development of lithium ion battery and its application on electrical vehicle (EV) and hybrid electrical vehicle (HEV). Manufacturer of both lithium ion battery and EV need a better understanding of lithium ion battery capacity fading mechanism, and have a major interest in predicting and improving the cycle life of lithium ion battery [1]. Many Battery management systems use battery open circuit voltage (OCV, can be obtained by discharging the battery at significantly low current) to predict the state of charge (SOC) of battery [2,3], however OCV–SOC curve of battery changes with battery capacity fading, leading to inaccurate estimation of SOC for cycled battery if the estimation is based on the original OCV–SOC curve. So the prediction of OCV–SOC curve of cycled battery is necessary for more accurate SOC estimation. The capacity fading of lithium ion battery is caused by several different mechanisms associate with side reactions, leading to electrolyte decomposition, passive film formation, active material dissolution, and other phenomena [4]. Recent investigations on lithium iron phosphate battery [5] reveals that battery capacity is affected by the battery temperature, depth of discharge (*DOD*) and operating current density.

In order to verify capacity fading mechanisms and predict capacity fading within battery, capacity fading models (Electrochemical model [4], Empirical correlations [6]; Equivalent circuit model [7]) have been presented by researchers. We are interest in electrochemical models and empirical correlations in this paper. Electrochemical models incorporate capacity fading governing equations to account for the capacity fading effect of battery using first principle model introduced by Doyle et al. [8]. Arora et al. [4]

* Corresponding author. Tel.: +65 65162207; fax: +65 67791459.
E-mail addresses: A0086270@nus.edu.sg (Y. Ye), mpetayao@nus.edu.sg (A.A.O. Tay).

0378-7753/$ – see front matter © 2012 Elsevier B.V. All rights reserved.
http://dx.doi.org/10.1016/j.jpowsour.2012.06.055

incorporated multiple capacity fading mechanisms into battery electrochemical model, and suggested another model [9] considering the lithium deposition overcharge reaction only in lithium ion battery with carbon-based negative electrode, the growth of SEI layer is implemented into an electrochemical model. SEI layer has been widely adopted by researchers [10,11]. Empirical correlations are developed by fitting capacity fading rate as a function of factors that affect the capacity fading based on a large amount of experiment data. Wang et al. [6] developed a cycle life model by fitting capacity fading as a function of battery temperature, current density and DOD based on comprehensive experimental data [5].

Electrochemical model considering all the capacity fading mechanisms has been proved to be efficient in validating capacity fading mechanisms as discussed above, but for predicting the rate of capacity loss, it turns out to be tedious work and it is difficult to find out the proportion that each mechanism contributes to the battery capacity loss and to keep a balance among them [12]. Therefore, when the focus is on predicting the rate of capacity loss, implementing the dominant capacity fading mechanism into electrochemical model would be more efficient than incorporating all the mechanisms. Empirical correlations [6] is straightforward in predicting capacity fading rate by fitting capacity fading rate as a function of battery operating conditions (such as temperature, current and DOD), however, such correlations are unable to predict corresponding battery discharging performance and OCV curve (which is essential for SOC prediction). In this work, we try to predict battery cycle life and battery discharging performance as well as OCV in one model by taking advantages of both electrochemical model and empirical correlations of battery cycle life. In order to take into account of the temperature effect on capacity fading, an electro-thermal model is developed than electrochemical model. Capacity fading mechanism is simplified that the dominant mechanism (active lithium loss) is chose to account for the overall capacity fading process, and experimental results [5] and correlations [6] are incorporated into the electro-thermal model, forming an electro-thermal cycle life model for lithium ion battery. The electro-thermal performance of this model is validated by experimental data from literature [13,14], and the cycle life prediction is validated by experimental data from Wang et al. [6]. The feasibility of using the dominant mechanism to account for the overall capacity fading process is verified and the effect of operating temperature on capacity fading rate is evaluated by the model. The model can be used for predicting discharging performance and OCV of cycled battery, and potential design consideration and capacity renovation methods are suggested and discussed.

2. Model development

2.1. Electrochemical part

The electrochemical model for $LiFePO_4$ lithium ion battery in this paper is developed based on the pseudo two-dimensional model of Doyle et al. [8,15,16], and has been presented in our previous work [16]. Fig. 1 shows a schematic calculation domain of one-dimensional (1D) battery model [8,15,17]. Two inner boundaries (Anode/separator interface boundaries 2 and cathode/separator interface boundaries 3) and two external boundaries (anode/current collector interface boundary 1 and cathode/current collector interface boundary 4) are shown in the figure. The spirally wound cylindrical battery is considered as a lumped single cell, so electrochemical performance is assumed to be homogeneous within the cylindrical battery. Average battery temperature T_{avg} in the 2D thermal model is feedback to the electrochemical model to account for the temperature effect on electrochemical performance of battery, heat generation rate Q_{avg} is in return a feedback from electrochemical model to thermal model for calculating the battery temperature.

2.1.1. Electronic charge balance

2.1.1.1. (a). Solid phase. Electronic charge balance for solid phase can be expressed as

$$\nabla\cdot\left(-\kappa_1^{\text{eff}}\nabla\phi_1\right) = -S_{\text{a,i}}j_{\text{loc,i}} \tag{1}$$

$$S_{\text{a,i}} = \frac{3\varepsilon_{1,\text{i}}}{r_{\text{p,i}}};\ \kappa_1^{\text{eff}} = \kappa_1\varepsilon_1^{\gamma_1} \tag{2}$$

where, ϕ_1 is arbitrarily set at zero at boundary 1; At boundary 4, the charge flux is set to be equal to the local current density I; At boundary 2 and boundary 3 are set as isolation, since there is no charge flux, Eq. (4).

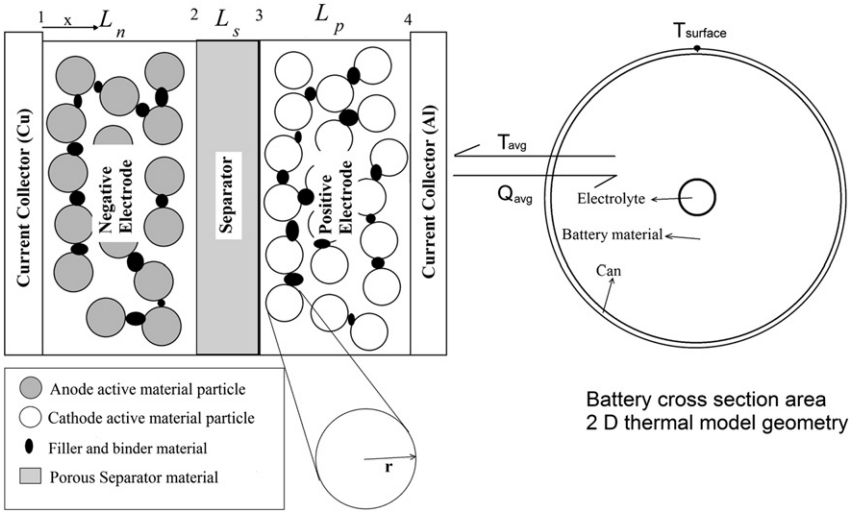

Fig. 1. Schematic of electro-thermal model geometry.

$$\phi_1|_{x=0} = 0;\ -\kappa_1^{\text{eff}}\nabla\phi_1\Big|_{x=L_n+L_s+L_p} = -I \tag{3}$$

$$-\kappa_1^{\text{eff}}\nabla\phi_1\Big|_{x=L_n+L_s} = 0;\ -\kappa_1^{\text{eff}}\nabla\phi_1\Big|_{x=L_n} = 0 \tag{4}$$

2.1.1.2. (b). Solution phase. The electronic charge balance governing equation in solution phase is expressed as:

$$\nabla\cdot\left\{\kappa_2^{\text{eff}}\left[-\nabla\phi_2 + \frac{2RT}{F}\left[1+\frac{\partial \ln f}{\partial \ln c_2}\right](1-t_+)\frac{\nabla c_2}{c_2}\right]\right\} = S_{\text{a,i}}j_{\text{loc}} \tag{5}$$

$$\kappa_2^{\text{eff}} = \kappa_2\varepsilon_2^{\gamma_2} \tag{6}$$

Liquid-junction potential is introduced in Eq. (5) with expression

$$K_{\text{junc}} = \frac{2RT}{F}\left[1+\frac{\partial \ln f}{\partial \ln c_2}\right](1-t_+) = \frac{2RT}{F}\nu \tag{7}$$

where ν is the thermodynamic factor relating to electrolyte activity, it is temperature and concentration dependent.

ϕ_2 is taken to be continuous at inner boundaries (boundary 2 and boundary 3), while it is set to be isolate boundary at external boundaries (boundary 1 and boundary 2) since there is no flux at these boundaries, Eq. (8).

$$\frac{\partial\phi_2}{\partial x}\Big|_{x=0} = \frac{\partial\phi_2}{\partial x}\Big|_{x=L_n+L_s+L_p} = 0 \tag{8}$$

2.1.2. Mass balance

2.1.2.1. (a). Solid phase. The mass balance of lithium ions in an intercalation particle of electrode active material is described by Fick's law. y is the distance from the center of solid sphere, the mass transport within solid phase can be described as:

$$\frac{dc_1}{dt} + \frac{\partial}{\partial y^2}\left(-y^2 D_{1,\text{i}}\frac{\partial}{\partial y}(c_1)\right) = 0 \tag{9}$$

where r_p is the particle radius. The lithium concentration at the surface of the particles, $y = r_p$, is coupled to the concentration and flux in the 1D model for the charge and material transport in the electrolyte. The flux at the center of sphere, $y = 0$, is set to zero, because there is no species source.

2.1.2.2. (b). Solution phase. Solution phase material balance for LiF_6 dissolved in the liquid phase

$$\varepsilon_2\frac{dc_2}{dt} + \nabla\cdot\left\{-D_2^{\text{eff}}\nabla c_2\right\} = \frac{S_{\text{a,i}}j_{\text{loc,i}}}{F}(1-t_+) \tag{10}$$

$$D_2^{\text{eff}} = D_2\varepsilon_2^{\gamma_2} \tag{11}$$

The flux of liquid species is set to zero at external boundaries (boundary 1 and 4), liquid species flux and species concentration are taken to be continuous at inner boundaries (boundary 2 and boundary 3).

2.1.3. Electrochemical kinetics

The local current per active material area is calculated using the Bulter–Volmer equation:

$$j_{\text{loc,i}} = i_{0,\text{i}}\left\{\exp\left(\frac{\alpha_{\text{a,i}}\eta_{\text{i}}F}{RT}\right) - \exp\left(\frac{-\alpha_{\text{c,i}}\eta_{\text{i}}F}{RT}\right)\right\} \tag{12}$$

where, $j_{\text{loc,i}}$ is driven by overpotential, η_{i}, defined as the difference between solid and electrolyte phase potentials minus U, the thermodynamic equilibrium potential of the solid phase.

$$\eta_{\text{i}} = \phi_{1,\text{i}} - \phi_{2,\text{i}} - U_{\text{ref,i}} \tag{13}$$

where the equilibrium potential, U, is taken to be a function of the solid phase lithium ion concentration at the particle surface. The temperature-dependent open circuit potential of electrode i is approximated by Taylor's first order expansion around a reference temperature:

$$U_{\text{i}} = U_{\text{ref,i}} + \left(T - T_{\text{ref}}\right)\frac{dU_{\text{i}}}{dT} \tag{14}$$

where $U_{\text{ref,i}}$ is the open circuit potential under the reference temperature.

In Eq. (12), exchange current density, $i_{0,\text{i}}$, acts as a bridge connecting concentrations in both solid phase as liquid phase:

$$i_{0,\text{i}} = Fk_{0,\text{i}}c_2^{\alpha_c}\left(c_{1,\max,\text{i}} - c_{1,\text{surf,i}}\right)^{\alpha_c}c_{1,\text{surf,i}}^{\alpha_a} \tag{15}$$

where $k_{0,\text{i}}$ is a reaction rate, considered temperature dependent in this paper. α_a and α_c are the anodic and cathodic transfer coefficients, respectively.

The outputs of the model are the cell potential, current density distribution, species and concentrations distributions. The cell potential is derived by following expression:

$$E = \phi_1|_{x=L_n+L_s+L_p} - \phi_1|_{x=0} \tag{16}$$

2.2. Thermal model

There are 3 domains in the 2D thermal model geometry in Fig. 1: 1. Battery core filled with electrolyte; 2. Battery body filled with battery material (electrodes, current collectors and separator); 3. Metal can. There is heat generated in the battery body, but not in battery core and metal can. The volume averaged heat generation rate Q_{avg} in battery body, as shown in Fig. 1,is the sum of the local heat generation from electrochemical model, including reaction heat generation Q_{rea}, ohmic heat generation Q_{ohm} and active heat generation Q_{act}, heat generation in current collector is neglected because the electrical conductivities of current collectors are significantly larger than that of electrode materials that heat generated in current collectors is much smaller than in electrodes.

Active heat generation is:

$$Q_{\text{act}} = S_{\text{a,i}}j_{\text{loc,i}}(\phi_{1,\text{i}} - \phi_{2,\text{i}} - U_{\text{i}}) \tag{17}$$

Reaction heat generation is:

$$Q_{\text{rea}} = S_{\text{a,i}}j_{\text{loc,i}}T\frac{\partial U_{\text{i}}}{\partial T} \tag{18}$$

Ohmic heat generation is:

$$Q_{\text{ohm}} = \sigma^{\text{eff}}\nabla\phi_1\cdot\nabla\phi_1 + \kappa^{\text{eff}}\nabla\phi_2\cdot\nabla\phi_2 + \kappa_D^{\text{eff}}\frac{\nabla c_{\text{e}}}{c_{\text{e}}}\cdot\nabla\phi_2 \tag{19}$$

So the volume averaged heat generation rate is

$$Q_{avg} = Q_{act} + Q_{rea} + Q_{ohm} \quad (20)$$

The energy balance of the 2D geometry is shown as follows:

$$\rho C_p \frac{\partial T}{\partial t} + \nabla \cdot (-k \nabla T) = Q_{avg}$$

ρ, C_p and k are the volume averaged density, heat capacity and thermal conductivity, respectively.

According to Newton's cooling law and radiation law, the boundary condition for energy balance is expressed as:

$$-\lambda \frac{\partial T}{\partial x} = -h(T_{amb} - T) - \varepsilon\left(T_{amb}^4 - T^4\right) \quad (21)$$

where h is lumped heat transfer coefficient, T_{amb} is the ambient temperature, and ε is the blackness of the battery surface ($\varepsilon = 0.8$ [18]).

2.3. Capacity fading part

The capacity of lithium ion battery is limited by the amount of active lithium [5]. The instability of carbon negative/electrolyte interface is suspected to be the source of active lithium loss. However, there is slight change in the positive electrode [5]. This paper focuses on predicting discharging performance and OCV of cycled battery in a simple way, so we incorporate only the dominant mechanism (active lithium loss) into the model for cycle life prediction, the feasibility of such simplification will be discussed later. Therefore, in this model, the change of amount of active lithium (dominant mechanism) is expressed by varying the initial state of charge ($SOC_{0,n}$) of negative electrode to account for the battery capacity fading process.

As mentioned above, Wang et al. [6] provided a function of capacity fading rate of 26,650 cylindrical lithium iron phosphate during C/2 discharging at different ambient temperature.

$$Q_{loss} = 30330\exp\left(\frac{-31500}{8.314T}\right)A_h^{0.552} \quad (22)$$

In this work, the above function is integrated into $SOC_{0,n}$ to account for the capacity fading effect in the electro-thermal model.

$$SOC_{0,n,N} = SOC_{o,n}\left(1 - 30330\exp\left(\frac{-31500}{8.314T}\right)A_h^{0.552}\right) \quad (23)$$

where A_h is expressed as

$$A_h = (\text{cycle\_number}) \times (\text{DOD}) \times (\text{full\_cell\_capacity}) \quad (24)$$

By imputing the cycle number N, this model would be able to calculate the capacity loss of battery.

3. Model parameters and model validation

3.1. Model calibration

3.1.1. Model parameters

The calculations of model were performed using the finite element commercial software COMSOL MULTIPHYSICS® (Version 3.5a). Model parameters are from manufacturer's data, literature and estimation. Parameters for a 2.3 Ah $LiFePO_4$ battery are listed in Tables. 1 and 2, including design specifications, lithium ion concentration parameters, Kinetic and transport properties and thermal properties. Kinetic reaction rate constant at reference temperature of cathode ($k_{0,p}$) in Table 1 is estimated by matching the simulated discharge potential with experiment data. Specific heat capacity and density of the battery body in Table 2 are the volume averaged value of electrode materials, current collectors and separator. Bulk thermal conductivity is experimentally measured to be 0.2 W(m K)$^{-1}$ rather than using the volume averaged value because there are contact resistances which are difficult to measure between two different layer of battery materials.

Table 1
Model parameter for a 2.3 Ah $LiFePO_4$ cylindrical 26650 type battery electrochemical sub-models.

	Anode	Separator	Cathode
Design specifications (geometry and volume fractions)			
A_{cell} (m^2)	0.1694[a]		
$\varepsilon_{1,i}$	0.55[a]	–	0.43[a]
$\varepsilon_{2,i}$	0.33[a]	0.54[a]	0.332[a]
L_i (μm)	34[a]	30[a]	70[a]
R_i (μm)	0.0365[a]	–	3.5[a]
Lithium ion concentrations			
C_{20} (mol m^{-3})	1200[a]		
$C_{max,i}$ (mol m^{-3})	31370[b]	–	22806[b]
$SOC_{0,i}$	0.8[b]	–	0.03[b]
Kinetic and transport properties			
$\alpha_{a,i}$, $\alpha_{c,i}$	0.5	–	0.5
γ_i	1.5	1.5	1.5
D_2 (m^2 s^{-1})	Eq. (25)		
$D_{10,i}$ (m^2 s^{-1})	3.9×10^{-14}[c]	–	1.18×10^{-18}[b]
$E_{a,D,i}$ (kJ mol^{-1})	35[d]	–	35[b]
$k_{0,i}$ ($m^{2.5}$ $mol^{-0.5}$ s^{-1})	3×10^{-11}[e]	–	1.4×10^{-12}[f]
$E_{a,k,i}$ (kJ mol^{-1})	20[g]	–	30[b]
κ_1 (S m^{-1})	100[c]	–	0.5[h]
κ_2 (S m^{-1})		Eq. (26)	
t^+	0.363[c]		
ν	Eq. (27)		
T_{ref} (K)	298.15		
F (C mol^{-1})	96,487		

[a] Manufacturer.
[b] Ref. [13].
[c] Ref. [19].
[d] Ref. [20].
[e] Ref. [21].
[f] Estimate.
[g] Ref. [22].
[h] Ref. [23].

3.1.2. Temperature dependent parameters

The data of lithium ion diffusivity in solution phase D_2, electric conductivity in solution phase κ_2 and thermodynamic factor ν are adopted from published literature Ref. [28]. The solvent mixture for the commercial battery tested is unknown, but we assume that Eqs. (25)–(27) are applicable in this commercial battery and use these data in our calculation even though the solvent mixture of the battery might be different from that in [28]:

Table 2
Thermal properties for a 2.3 Ah $LiFePO_4$ cylindrical 26650 type battery.

Thermal properties	k_i (W(m K)$^{-1}$)	ρ_i (kg m^{-3})	Cp_i (J(kg K)$^{-1}$)
Anode	1.04[a]	2500[b]	800[b]
Separator	1[a]	1200[b]	800[b]
Cathode	1.48[a]	1500[b]	800[b]
Cu	401	8900	3440
Al	237	2700	2420
Battery material	0.2[c]	2101	1014
Volume averaged			
Electrolyte	0.6[d]	1130[d]	2055[d]
Can	14[e]	7500[e]	460[e]

[a] Ref. [24].
[b] Ref. [25].
[c] Measure.
[d] Ref. [26].
[e] Ref. [27].

$$D_2 = 1\times10^{-4}10^{-4.43-\frac{54.0}{T-229.0-0.005c}-2.2\times10^{-4}c} \quad (25)$$

$$\begin{aligned}\kappa_2 = {} & 1\times10^{-4}c\Big(-10.5+0.074T-6.69\times10^{-5}T^2\\ & +6.68\times10^{-4}c-1.78\times10^{-5}cT\\ & +2.8\times10^{-8}cT^2+4.94\times10^{-7}c^2\\ & -8.86\times10^{-10}c^2T\Big)^2\end{aligned} \quad (26)$$

$$\begin{aligned}\nu = {} & 0.601-0.24\sqrt{10^{-3}c}\\ & +0.982\left[1-0.0052(T-294.0)\sqrt{10^{-9}c^3}\right]\end{aligned} \quad (27)$$

Diffusivity coefficient and reaction rate constants follow the following Arrhenius formula [29]:

$$A_i = A_{0,i}\exp\left(\frac{E_{a,i}}{R}\left(\frac{1}{T_{ref}}-\frac{1}{T}\right)\right) \quad (28)$$

$$D_{1,n} = 3.9\times10^{-14}\exp\left(\frac{35000}{R}\left(\frac{1}{298.15}-\frac{1}{T}\right)\right) \quad (29)$$

$$D_{1,p} = 1.18\times10^{-18}\exp\left(\frac{35000}{R}\left(\frac{1}{298.15}-\frac{1}{T}\right)\right) \quad (30)$$

$$k_{1,n} = 3\times10^{-11}\exp\left(\frac{20000}{R}\left(\frac{1}{298.15}-\frac{1}{T}\right)\right) \quad (31)$$

$$k_{1,p} = 1.4\times10^{-12}\exp(-3\bar{y})\exp\left(\frac{30000}{R}\left(\frac{1}{298.15}-\frac{1}{T}\right)\right) \quad (32)$$

In order to match the simulation result with experimental data, we add a ratio of $\exp(-3\bar{y})$ into the formula of reaction rate of positive electrode. This ratio is specific to our model, and does not necessarily apply to other models.

3.1.3. Electrode thermodynamic properties

State of charge (SOC) of $Li_{\bar{x}}C_6$ negative electrode is:

$$SOC_n = \bar{x} = c_{1,n}/c_{1,max,n} \quad (33)$$

And state of charge of $Li_{\bar{y}}FePO_4$ positive electrode is:

$$SOC_p = \bar{y} = c_{1,p}/c_{1,max,p} \quad (34)$$

The open circuit potential of negative electrode U_n and positive electrode U_p are from Ref. [13], Fig. 2. Point B is the characteristic point of open circuit potential curve of negative electrode (U_n), DE is the effective SOC range of positive electrode, and AC is the effective SOC range of negative electrode.

Lithium graphite entropy is from Ref. [23]:

$$\frac{dU_n}{dT} = 344.1347148\frac{\exp(-32.9633287\bar{x}+8.316711484)}{1+749.0756003\exp(-34.7909964\bar{x}+8.887143624)}-0.8520278805\bar{x}+0.36229929\bar{x}^2+0.2698001697 \quad (35)$$

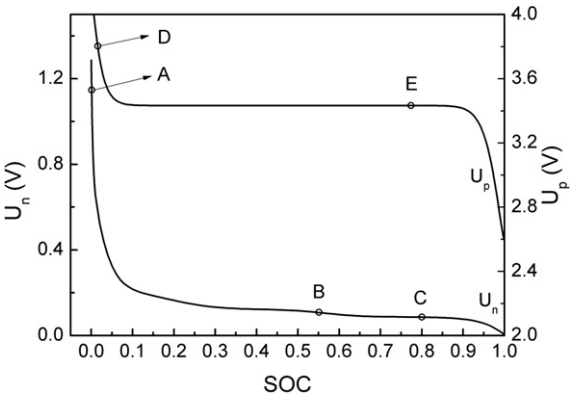

Fig. 2. Open circuit potential of positive electrode (U_p) and negative electrode (U_n).

Lithium iron phosphate entropy is also from Ref. [23] :

$$\begin{aligned}\frac{dU_p}{dT} = {} & -0.35376\bar{x}^8+1.3902\bar{x}^7+1.9635\bar{x}^5-0.98716\bar{x}^4\\ & +0.28857\bar{x}^3-0.046272\bar{x}^2+0.0032158\bar{x}\\ & -1.9186\times10^{-5}\end{aligned} \quad (36)$$

3.2. Model validation

This electro-thermal cycle life model is validated from electrochemical performance, thermal performance and cycle life perspective. Experimental data are from different experiment done by different researchers [6,13,14] with the same type of battery (26650C lithium iron phosphate battery, 2.3 Ah).

3.2.1. Electrochemical performance

The electro-thermal cycle life model is first validated from the electrochemical performance perspective. Experiment data of battery potential against discharge capacity at different ambient temperature (0 °C [6], 25 °C [13], 45 °C [6,13], 60 °C [6]) with C/2 current are compared with the simulation results. The good agreements in Fig. 3 shows that this electro-thermal cycle life model is able to simulate battery discharge performance at different ambient temperature. To further validate the electrochemical performance during charge and discharge with different current density, the simulation results are compared with the experiment data [13] of battery charge and discharge with different current density (C/10, 1/2C, 1 C) at 45 °C in Fig. 4 and Fig. 5, respectively.

3.2.2. Thermal characterization

Forgez et al. [14] experimentally measured the battery surface temperature and center temperature during 6 C constant current charge–constant voltage charge–constant current discharge process (CC–CV–CC). To evaluate the thermal performance of the electro-thermal cycle life model, the current profile of Forgez et al. [14] is implemented into the model for simulation. The comparison of simulation results with experiment data is shown in Fig. 6. The

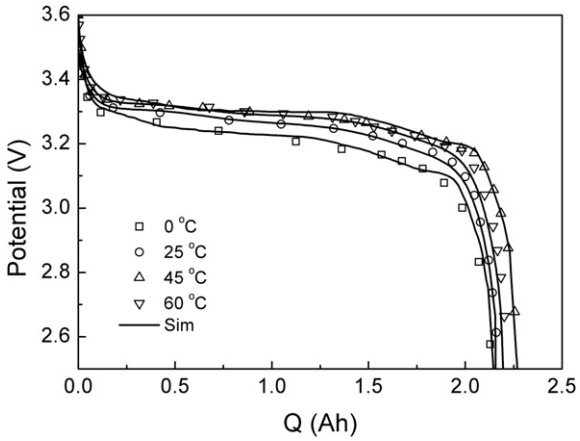

Fig. 3. 0 °C [6], 25 °C [13], 45 °C [6,13], 60 °C [6], C/2 discharge validation.

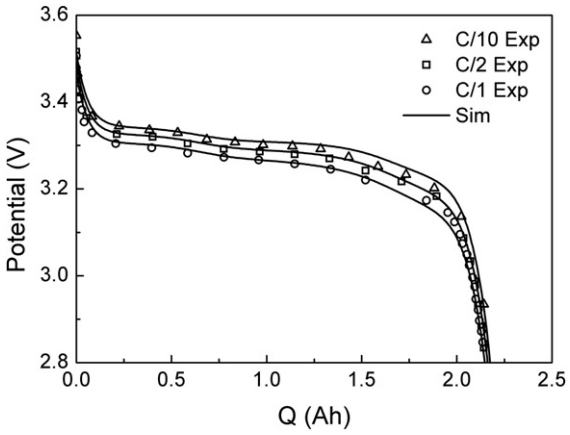

Fig. 5. Different *C*_rate (C/10, 0.5C, 1C) discharge validation at 45 °C [13].

experimental data of temperature include the center temperature of battery measured by a thermal couple inserted into the center of the battery, and the surface temperature measured by a thermal couple stuck to the battery surface [14]. Temperature decreases during the constant voltage charging period, probably because there is lower heat generation rate during that period than constant current charging period and constant current discharging period. The simulation results agree well with experimental data during the CC–CV–CC process, showing that this model is capable of predicting battery temperature.

3.2.3. Capacity fading validation

Finally, the simulation results of discharge performance at different ambient temperature and different cycle number are validated against the experiment data from Wang [6], Fig. 7 and Fig. 8. It has to be mentioned that the cycle life function implemented in this electro-thermal model is also adopted from the work of Wang [6]. Therefore the accuracy of capacity prediction in this model (related to the end point correspond to the discharge end) would be the same as the function of Wang's. However, the good agreement of discharge curve shapes is ensured by the implementing method of capacity fade function into the model, this method would be further discussed in the following section.

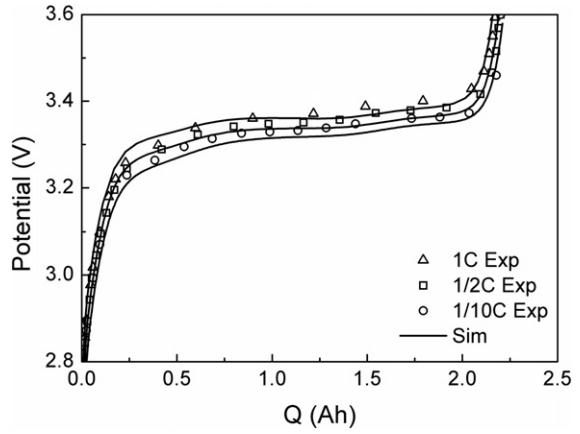

Fig. 4. Different *C*_rate (C/10, 0.5C, 1C) charge validation at 45 °C [13].

4. Results and discussion

4.1. Assumption validation and OCV prediction

As we assume that the dominant factor of capacity fading can represent the overall capacity fading phenomenon, and we use the variation of $SOC_{0,n}$ alone to simulate the capacity fading in the model for the sake of simplicity, though the discharging performances of cycled battery have been validated in the previous section, we still need to verify the feasibility of making the assumption more clearly. As shown in Fig. 9, the simulation result of discharging potential of 0.5 C cycled 272 times at 45 °C matches well with the experiment data. The characteristic point A nearly overlap between simulation result and experiment data, while there is a slight discrepancy of the position of characteristic point B between simulation result and experiment data. The discrepancy of B may be due to our assumption of using the dominant factor to represent the overall capacity fading phenomenon. However, as far as discharging potential is concerned, the small discrepancy in discharging potential is acceptable.

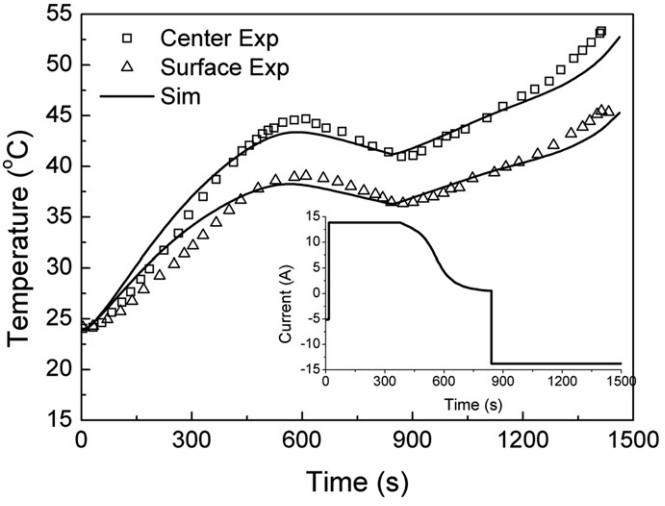

Fig. 6. Surface temperature and center temperature of battery during 6C (CC–CV–CC) charge and discharge [10].

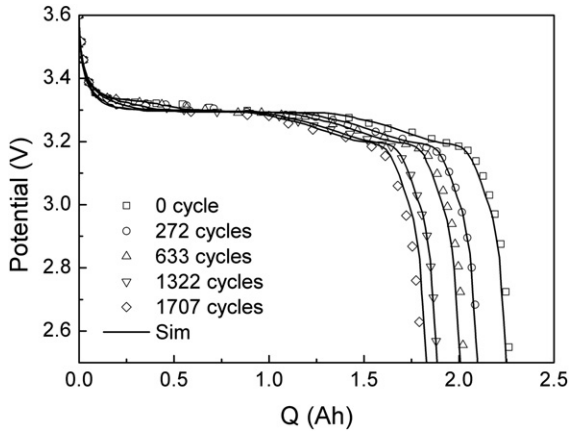

Fig. 7. Validation of capacity fading at 45 °C [6].

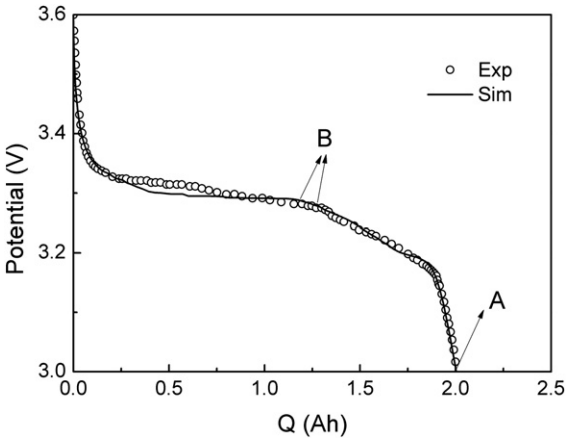

Fig. 9. 45 °C, 1/2 C_rate discharge, cycle number 272, verification of discharging potential.

As introduced before, OCV–SOC curve in BMS should be updated than the original one to ensure accuracy in SOC estimation. As OCV–SOC curve can be experimentally obtained by discharging the battery at low current, we try to simulate the OCV–SOC curves of cycled battery by discharging the battery with 1/50 C current in the model. Simulation results are shown in Fig. 10, the OCV curves of different cycle numbers differ a lot, which in return verify the significance of using updated OCV curves than the original one in BMS for SOC estimation.

4.2. Capacity recovering

As shown in Fig. 11, due to the loss of active lithium in cycled battery, for a fully discharged battery, the SOC of the positive electrode moves from E (the original position) to E_1, and for a fully charged battery, the SOC of the negative electrode moves from C (the original position) to C_1.

To recover the capacity in cycled battery, two methods can be utilized. When the cycled battery is fully charged (point C_1 in negative electrode and point D in positive electrode in Fig. 11), further charging is impossible since there is not further supply of lithium ions from positive electrode to negative electrode. Therefore, the first method is to charge the positive electrode alone from D to D_2, this charging process can be conduct by charging the positive electrode with a lithium metal electrode (lithium metal electrode acts as lithium ion source for positive electrode). After the process, the battery can be further charged, since there are more lithium ions in positive electrode to transport to the negative electrode. The final condition of fully charged battery is point D in positive electrode and point C_2 in negative electrode. And fully discharged battery is point E_2 in positive electrode and point A in negative electrode. Capacity before recovering is AC_1, and after recovering is AC_2, capacity of C_1C_2 is recovered to the battery. The schematic setup of the recovering process is shown in Fig. 12, a lithium metal electrode is connected with the positive electrode current collector of the disclosed battery by the external power supply and the same electrolyte as the battery. Lithium metal serves as the lithium ion sources and the electrolyte acts as a channel for lithium ions to transport to and insert into the positive electrodes. In this process, additional active lithium is supplied to the cycle battery.

On the other hand, when the battery is fully discharged (negative electrode at point A and positive electrode at E_1), the capacity is limited by the negative electrode that its SOC is 0 (point A) and cannot further provide lithium ions to insert into the positive electrode, Fig. 11. Therefore, another method for recovering battery capacity is to charge the negative electrode alone to move point A rightward to A_3, this process can be conduct by charging the negative alone with a lithium metal reference electrode. After this process, the battery can be further discharged, since there are more lithium ions in negative electrode to provide to insert into the positive electrode. The final condition of fully discharged battery can be point E_3 in positive electrode and point A in negative

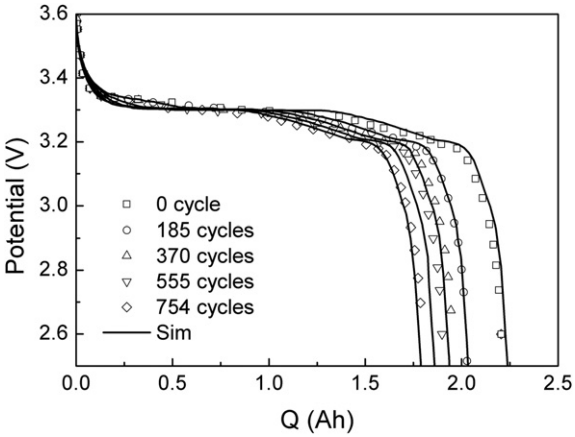

Fig. 8. Validation of capacity fading at 60 °C [6].

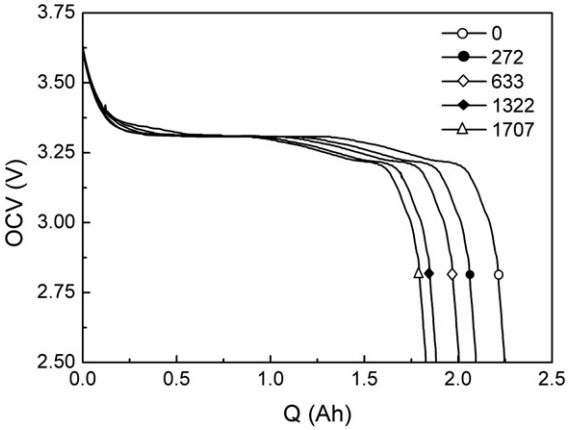

Fig. 10. Prediction of OCV of different cycles at 45 °C with 0.5C current.

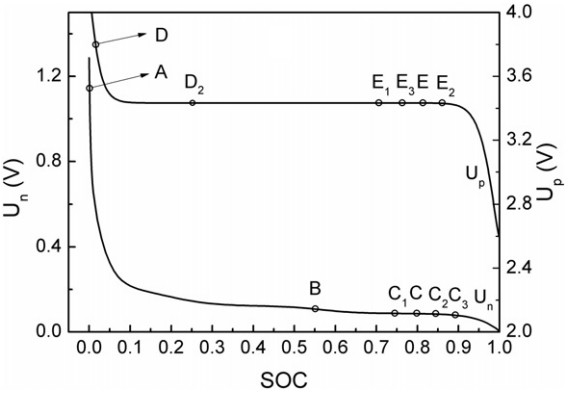

Fig. 11. Schematic of battery capacity fading and recovering.

electrode, and fully charged battery can be point D in positive electrode and point C_3 in negative electrode. Capacity before recovering is AC_1, and after recovering is AC_3, capacity of C_1C_3 is recovered to the battery. The schematic setup of the recovering process is shown in Fig. 13.

Considering the safety issue in the recovering process of capacity fade, charging the negative electrode of fully discharged battery would be a better choice than charging the positive electrode of fully charged battery, because short circuit or other hazards would cause more serious safety problem for fully charged battery than fully discharged battery. As shown in Fig. 14(a), the core of a cylindrical battery is filled with electrolyte, a lithium metal rode electrode can be inserted into the core, it would be possible especially for battery with larger diameter. Charging the negative electrode of a fully discharged battery may be realized by the setup sketched in Fig. 14(b).

4.3. Self-heating and temperature effect

Capacity fading rate is a function of temperature, while the battery temperature would be rose by the self-heating effect of battery, leading to higher temperature of battery and higher capacity fading rate. Capacity fading rate can be expressed as [8]:

$$Q_{\text{loss}} = B \cdot \exp\left(\frac{-E_a}{RT}\right)(A_h)^z \tag{38}$$

where the pre-exponent factor B decreases with increasing *C*_rate, but is difficult to quantitatively describe this relationship by using a simple mathematical correlation; The index number z is almost constant to 0.55; while the E_a decrease with increasing *C*_rate, and is fitted into a function of *C*_rate as follows [6]:

$$E_a = -31700 + 370.3 \times C\_\text{rate} \tag{39}$$

However, as a thermodynamic term for battery, E_a is supposed to be a constant rather than a function of *C*_rate. The decreasing trend of E_a with *C*_rate in Eq. (38) is deduced to the lower T value used in the function. Wang et al. [6] used the battery surface temperature in the Eq. (38), while the surface temperature may not be representative for the battery. Due to the high heat transfer coefficient around the battery surface in experiment, the surface temperature of the battery is close to the ambient air temperature, especially for those conditions in which the ambient air temperature is higher [6], such as 25 °C or 45 °C, while the temperature within battery differ from the surface temperature and is difficult to measure.

Simulation results (Fig. 15) of battery discharged with different *C*_rate at ambient temperature of 45 °C, and heat transfer coefficient h at 70 W m^{-2} K^{-1} show that the surface temperature of battery is generally lower than the average temperature, and the difference between battery surface temperature and average temperature increases with *C*_rate and discharge capacity as shown in Fig. 10. Therefore, battery surface temperature (T_{surface}) underestimates the battery temperature. To better capture the influence of temperature on the capacity fading, using the volume average temperature as a characteristic temperature would be a better choice, and the E_a in the capacity function is likely to be a constant at different discharging *C*_rates. In sum, surface temperatures used

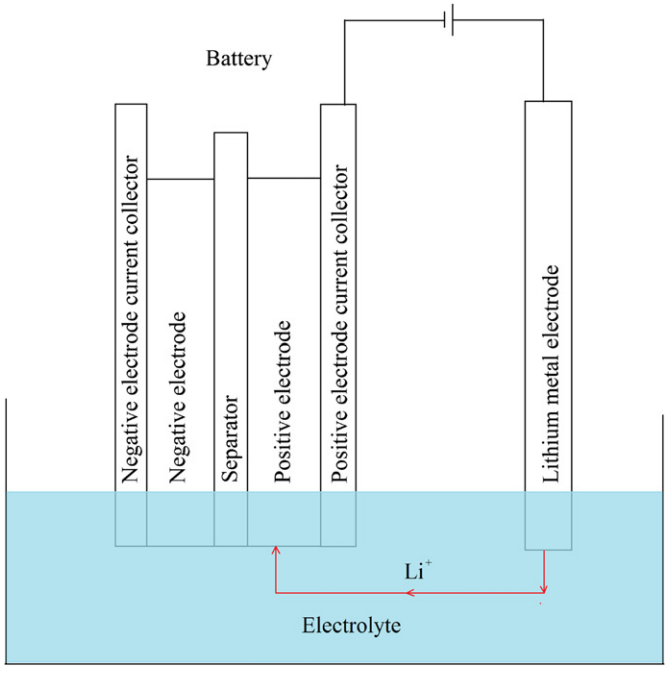

Fig. 12. Schematic setup of recovering battery capacity by charging positive electrodes.

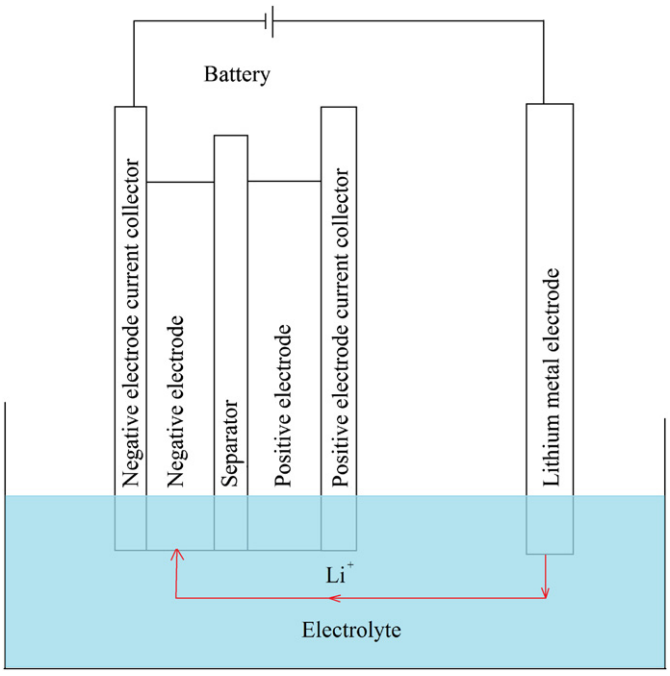

Fig. 13. Schematic setup of recovering battery capacity by charging negative electrodes.

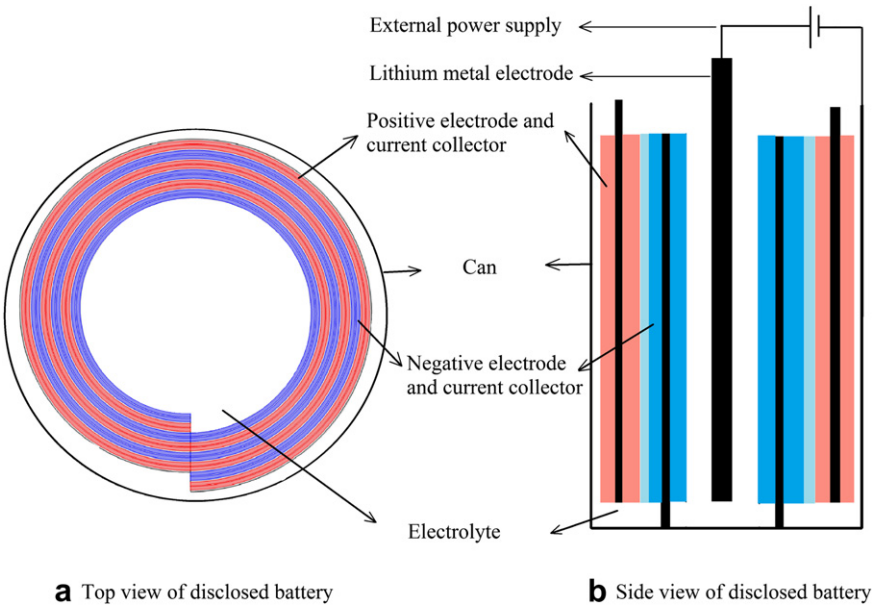

Fig. 14. Schematic setup of recovering cylindrical battery capacity by charging the negative electrodes.

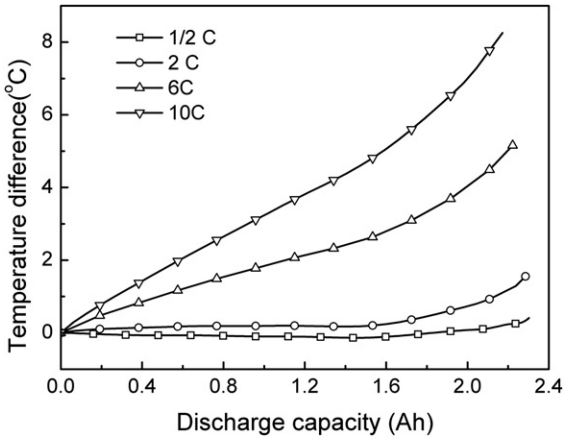

Fig. 15. Temperature difference between average temperature and surface temperature, $T_{avg}-T_{surface}$.

in in Wang's [6] capacity fading function underestimate the temperature effect of capacity fading rate. However, due to the measurement limitation, the measurable temperature is the surface temperature, it is a compromise to use the surface temperature as the characteristic temperature of the battery.

5. Conclusion

An electro-thermal cycle life model is develop by implementing capacity fading effect in electro-thermal model of cylindrical lithium ion battery, this model is able to simulate the discharging performance during different discharge cycles, predicting battery temperature, as well as predicting capacity loss at different cycle number. The electro-thermal cycle model is comprehensively validated in the aspects and the simulation results well agree with experimental data.

It is feasible to use the dominant factor to represent the overall capacity fading of battery for simplicity, and the accuracy of simulation results of discharging potential is acceptable. The model can be used to predict updated OCV curves which are necessary for accurate estimation of SOC for cycled battery in BMS.

To recover the capacity loss of cycled battery, additional lithium ion should be provided to the battery. Either charging the negative electrode of fully discharged battery or charging the positive electrode of fully charged battery, would be possible method to achieve active lithium compensation. Charging the negative electrode of fully discharged battery would be a better choice considering the safety issue. Possible capacity recovering setup has been proposed.

The temperature predicting capability is validated against the experimental data of battery surface temperature and center temperature during 6 *C*_rate constant current charge–constant voltage charge–constant current discharge (CC–CV–CC). Temperatures predicted by the model for different *C*_rate show that battery surface temperature underestimate the temperature of battery, the decreasing trend of *E*a with increasing *C*_rate is deduced to the increasing battery temperature with increasing discharge *C*_rate, and half radius temperature or volume average temperature would be a better parameter to characterize the battery temperature and would be able to better help evaluate temperature effect on capacity fading rate.

References

[1] S.S. Choi, H.S. Lim, J. Power Sources 111 (2002) 130–136.
[2] V. Pop, H.J. Bergveld, P. Notten, et al., Measurement 42 (2009) 1131–1138.
[3] C.P. Zhang, J.C. Jiang, W.G. Zhang, et al., Energies 5 (2012) 1098–1115.
[4] P. Arora, R.E. White, M. Doyle, J. Electrochem. Soc. 145 (1998) 3647–3667.
[5] P. Liu, J. Wang, J. Hicks-Garner, E. Sherman, et al., J. Electrochem. Soc. 157 (2010) A499–A507.
[6] J. Wang, P. Liu, J. Hicks-Garner, et al., J. Power Sources 196 (2011) 3942–3948.
[7] I.S. Kim, IEEE Trans. Power Electron. 25 (2010) 1013–1022.
[8] M. Doyle, T.F. Fuller, J. Newman, J. Electrochem. Soc. 140 (1993) 1526–1533.
[9] P. Arora, M. Doyle, R.E. White, J. Electrochem. Soc. 146 (1999) 3543–3553.
[10] G. Ning, R.E. White, B.N. Popov, Electrochim. Acta 51 (2006) 2012–2022.
[11] P. Ramadass, B. Haran, P.M. Gomadam, R. White, et al., J. Electrochem. Soc. 151 (2004) A196–A203.
[12] M. Safari, C. Delacourt, J. Electrochem. Soc. 158 (2011) A1436–A1447.
[13] M. Safari, C. Delacourt, J. Electrochem. Soc. 158 (2011) A562–A571.
[14] C. Forgez, D.V. Do, G. Friedrich, et al., J. Power Sources 195 (2010) 2961–2968.
[15] T.F. Fuller, M. Doyle, J. Newman, J. Electrochem. Soc. 141 (1994) 1–10.
[16] Y. Ye, Y. Shi, N. Cai, et al., J. Power Sources 199 (2012) 227–238.
[17] K.A. Smith, C.D. Rahn, C.Y. Wang, IEEE T. Contr. Syst. T. 18 (2010) 654–663.
[18] X.W. Zhang, Electrochim. Acta 56 (2011) 1246–1255.

[19] S. Santhanagopalan, Q.Z. Guo, P. Ramadass, R.E. White, J. Power Sources 156 (2006) 620–628.
[20] O.Y. Egorkina, A.M. Skundin, J. Solid State Electrochem. 2 (1998) 216–220.
[21] K. Kumaresan, G. Sikha, R.E. White, J. Electrochem. Soc. 155 (2008) A164–A171.
[22] T.L. Kulova, A.M. Skundin, E.A. Nizhnikovskii, et al., Russ. J. Electrochem. 42 (2006) 259–262.
[23] R.E. Gerver, J.P. Meyers, J. Electrochem. Soc. 158 (2011) A835–A843.
[24] C. Lin, K. Chen, F. Sun, P. Tang, et al., Research on Thermo-physical Properties Identification and Thermal Analysis of EV Li-ion Battery, Vehicle Power and Propulsion Conference, Dearborn, MI, 2009, 1643–1648.
[25] V. Srinivasan, C.Y. Wang, J. Electrochem. Soc. 150 (2003) A98–A106.
[26] S.C. Chen, Y.Y. Wang, C.C. Wan, J. Electrochem. Soc. 153 (2006) A637–A648.
[27] T.D. Hatchard, D.D. MacNeil, A. Basu, et al., J. Electrochem. Soc. 148 (2001) A755–A761.
[28] L.O. Valoen, J.N. Reimers, J. Electrochem. Soc. 152 (2005) A882–A891.
[29] D. Bernardi, E. Pawlikowski, J. Newman, J. Electrochem. Soc. 132 (1985) 5–12.

Nomenclature

A_{cell}: area of the positive (both sides) that has opposing negative (m^2)
$c_{1,i}$: reduced-lithium in active material (mol m^{-3})
$C_{1,max,i}$: maximum concentration (mol m^{-3})
$C_{p,i}$: heat capacity $(J(kg\ K)^{-1})$
$D_{1,i}$: solid phase diffusivity ($m^2\ s^{-1}$)
$D_{10,i}$: solid phase diffusivity at reference temperature ($m^2\ s^{-1}$)
$E_{a,D,i}$: active energy for diffusion (kJ mol^{-1})
$E_{a,k,i}$: reaction active energy (kJ mol^{-1})
h: heat transfer coefficient (W $m^{-2}\ K^{-1}$)
I: cell current density based on A_{cell} (A m^{-2})
$j_{0,i}$: exchange current density (A m^{-2})
$j_{loc,i}$: local current density (A m^{-2})
$k_{0,i}$: reaction rate constant ($m^{2.5}\ mol^{-0.5}\ s^{-1}$)
k_i: thermal conductivity $(W(m\ K)^{-1})$
L_i: thickness (μm)
N: cycle number
Q_{act}: active heat generation (W m^{-3})
Q_{ohm}: ohmic heat generation (W m^{-3})
Q_{rea}: reaction heat generation (W m^{-3})
Q_{loss}: ratio of capacity loss over full cell capacity
r: radius distance variable of particle (m)
r_p: characteristic particle radius of electrode particles (μm)
$S_{a,i}$: specific surface area (m^{-1})
$SOC_{0,i}$: initial state of charge
t: time (s)
t_+: transference number of Li ion species dissolved in liquid
T: absolute temperature (K)
T_{amb}: ambient temperature (K)
U: thermodynamic, open circuit voltage (V)
v: thermodynamic factor relating to electrolyte activity
x: distance variable through a cell component (m)
y: dimensionless radial distance of particles
$\overline{x}$: average composition variable of Li in $Li_{\overline{x}}C_6$
$\overline{y}$: average composition variable of Li in $Li_{\overline{y}}FePO_4$

Greek letters
$\alpha_{a,i}$: transfer coefficient for anodic current
$\alpha_{c,i}$: transfer coefficient for cathodic current
ε: blackness of battery surface
$\varepsilon_{1,i}$: active material volume fraction
$\varepsilon_{2,i}$: volume fraction
ϕ_i: electric potential (V)
γ_i: Bruggeman tortuosity exponent
κ: ionic or electronic conductivity (S m^{-1})
ρ_i: density (kg m^{-3})
σ_i: solid phase conductivity (S m^{-1})

Subscripts, superscripts and acronyms
0: initial or equilibrated state
amb: ambient (temperature)
cell: battery
n: negative electrode
p: positive electrode
s: separator
ref: reference composition of relative to a Li/lithium ion reference electrode or reference temperature for Arrhenius formula